Universal functions for Burgers turbulence

Shadab Alam [1,*] P. K. Sahu [2,†] and Mahendra K. Verma [3,‡]
[1]Department of Mechanical Engineering, Indian Institute of Technology Kanpur, Kanpur 208016, India
[2]Department of Mathematics, Government Shyama Prasad Mukharjee College, Sitapur 497111, Chhattisgarh, India
[3]Department of Physics, Indian Institute of Technology Kanpur, Kanpur 208016, India

(Received 19 March 2022; accepted 6 July 2022; published 22 July 2022)

For the steady state of Burgers turbulence, Saffman [in *Topics in Nonlinear Physics* (Springer, Berlin, 1968), pp. 485–614] derived analytical expressions for the second-order structure function and energy spectrum in the inertial-dissipation range. By nondimensionalizing these quantities, we derive universal functions for the structure function and the energy spectrum and flux. We simulate Burgers turbulence with large-scale forcing for various injection rates and viscosity. For all these runs, the nondimensionalized structure functions and the energy spectra and fluxes collapse to the respective universal functions.

DOI: 10.1103/PhysRevFluids.7.074605

I. INTRODUCTION

The celebrated Burgers equation [1,2] is an important equation of nonlinear dynamics. It has been studied extensively because of its wide application, such as pressure-less gas dynamics [3], modeling vehicular traffic system [4], nonlinear acoustics [5–9], and cosmology (see [10,11] and the references therein). Using analytical tools, Saffman [12], Tatsumi and Kida [13], and Burgers [14] showed that, in the limit of vanishing viscosity and at large times, the asymptotic velocity field of Burgers turbulence can be expressed by a series of linear profiles separated by sharp jumps called *shocks*. Most of the energy dissipation occurs in these shocks because of strong velocity gradients [15–20].

Saffman [12] solved the Burgers equation analytically and derived the energy dissipation rate and root mean square (rms) velocity. He also computed the second-order structure function and energy spectrum, which is applicable to all lengthscales, that is, in the inertial range (larger than shock width) as well as dissipation range (less than or equal to shock width). In this paper, we generalize the Saffman's formulas to derive universal functions for Burgers turbulence. We also verify these universal functions using numerical simulations.

There are many more works on Burgers turbulence, but mostly for the inertial range. The analytical solution of Kida [15], computational results of decaying Burgers turbulence by Ohkitani and Dowker [21] and Tran and Dritschel [22], and closure studies of decaying Burgers turbulence by Gotoh and Kraichnan [16] and Gotoh [23] showed that the energy spectrum $E(k) \sim k^{-2}$ in the inertial range, where k is the wave number. They argued that the k^{-2} scaling of the energy spectrum is due to the presence of the shocks in the velocity field. Gupta and Scalo [9] observed the k^{-2} spectrum in the numerical study of decaying compressible turbulence. In addition, Gotoh [23], Bouchaud, Mézard, and Parisi [24], and Verma [17] computed the qth-order structure functions $S_q(r) = \langle |u(x+r,t) - u(x,t)|^q \rangle$ and found that all $S_q(r) \propto r^{\zeta_q}$ with exponent $\zeta_q = 1$, where

*Corresponding author: shadab@iitk.ac.in
†praveensahu173@gmail.com
‡mkv@iitk.ac.in

$u(x,t)$ and $u(x+r,t)$ are the velocity fields at points separated by distance r. The exponent ζ_q is independent of q; thus, Burgers turbulence exhibits intermittency.

Verma [17], Chekhlov and Yakhot [25], Hayot and Jayaprakash [26], Fleischer and Diamond [27], and Zhang and She [28] performed numerical simulations of Burgers turbulence forced with force spectrum of $k^{-2\alpha}$. Fleischer and Diamond [27] simulated Burgers turbulence for $\alpha = 0$ and obtained $E(k) \sim k^{-1}$. They argued that the k^{-1} spectrum (instead of k^{-2}) is due to the small scale white-noise forcing that inhibits shock formation. Chekhlov and Yakhot [25], Verma [17], and Zhang and She [28] studied the system for $\alpha = 1/2$ and found that Burgers turbulence resembles Kolmogorov turbulence [$E(k) \sim k^{-5/3}$] with constant energy flux $\Pi(k)$. Verma [17] observed that the energy flux remains constant for all $\alpha \geqslant 1/2$ and that the energy spectrum follows k^{-2} scaling for $\alpha \geqslant 3/2$. Thus, for $\alpha \geqslant 3/2$, the small scale forcing is insignificant to inhibit shock formation. Hayot and Jayaprakash [26] also studied the system for a range of α and observed the following spectrum:

$$E(k) \sim k^{-\beta}; \qquad \beta = 1 + \tfrac{4}{3}\alpha \tag{1}$$

for $-3/4 \leqslant \alpha \leqslant 1/2$; they also showed that $S_q(r)$ grows linearly for positive α, indicating strong intermittency in Burgers turbulence due to the shocks.

Girimaji and Zhou [29], Das and Moser [30], Ni, Shi, and Chen [31], Moradi, Teaca, and Anderson [32], Buzzicotti *et al.* [33], and Murray and Bustamante [20] simulated Burgers turbulence forced at large scales, and observed that $E(k)$ follows only k^{-2} scaling. Thus, the energy spectrum of Burgers turbulence is independent of the exponent α when the forcing is active only at large scales. However, the spectrum depends on α when the forcing wave number band extends to small scales [see Eq. (1)].

Most papers cited above focus on the inertial range. Shalimov [34] and Girimaji and Zhou [29] studied the energy spectrum in the dissipation range of Burger turbulence. They argued that Saffman's formula for the dissipation range overpredicted the spectrum. In this paper, we show that Saffman's formula (apart from a typographical error) is correct. The discrepancy between Girimaji and Zhou [29]'s numerical results and Saffman's formula was due to a typographical error. To derive the energy spectrum for the inertial-dissipation range of hydrodynamic turbulence, Pao [35] assumed that the ratio of the energy spectrum and energy flux is independent of viscosity. Using a similar assumption, Verma [36] derived an expression for the inertial-dissipation range of Burgers turbulence. Unfortunately, Verma's [36] formula differs from that of Saffman [12]. Shalimov [34] also derived a formula for the dissipation range of Burgers turbulence.

We remark that decaying Burgers turbulence has a similar behavior as forced Burgers turbulence. A critical difference, however, is that the energy decreases in time for decaying turbulence. Inviscid Burgers turbulence has a very different behavior. Ray *et al.* [37] and Murugan *et al.* [38] simulated the Galerkin-truncated inviscid Burgers equation with smooth initial conditions and observed strongly localized short-wavelength oscillations called *tygers*. Tygers grow with time, and the solution thermalizes asymptotically. Recently, Verma *et al.* [39] showed that the equilibrium state of the inviscid Burgers equation is delta-correlated noise. The energy spectrum for the equilibrium state is a flat spectrum (k^0).

The outline of the paper is as follows. In Sec. II, we present Saffman's formalism, as well as universal functions for Burgers turbulence. Our numerical procedure is described in Sec. III. In Sec. IV, we present the numerical verification of universal functions. We conclude the paper in Sec. V.

II. BURGERS TURBULENCE: SAFFMAN'S FORMULAS AND UNIVERSAL FUNCTIONS

A. Saffman's analytical formulas

The forced Burgers equation is

$$\frac{\partial u}{\partial t} + u\frac{\partial u}{\partial x} = \nu\frac{\partial^2 u}{\partial x^2} + F, \tag{2}$$

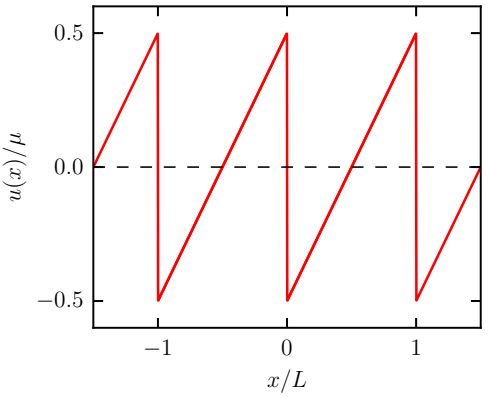

FIG. 1. At $\mathrm{Re} = 10^5$, the plot of the normalized velocity profile $u(x)/\mu$ versus x/L for Eq. (4).

where $u(x,t)$ is the velocity field, ν is the kinematic viscosity, and $F(x,t)$ is the random external force that injects energy into the system to maintain its steady state. Saffman [12] employed the following definition of the Reynolds number, Re, for Burgers turbulence:

$$\mathrm{Re} = \frac{\mu L}{\nu}, \tag{3}$$

where L is the length of the periodic domain and μ is the velocity jump across the shock, also called the shock strength. For $\mathrm{Re} \to \infty$ and $t \to \infty$ limit, Saffman [12] derived the following solution:

$$u(x) = \mu\left[-\frac{1}{2}\tanh\left(\frac{\mathrm{Re}}{4}\frac{x}{L}\right) + \frac{x}{L}\right]; \quad -\frac{L}{2} < x < \frac{L}{2}. \tag{4}$$

In Fig. 1, we plot $u(x)/\mu$ for $\mathrm{Re} = 10^5$. The figure shows that the velocity field is represented by a series of straight lines connected by sharp vertical shocks. The distance between two consecutive shocks is L (see Fig. 1), and the thickness of the shock δ is of the order of $4\nu/\mu$, which is the lengthscale of dissipation. In this paper, we readopt Saffman's formula for a box length of L (not $2L$, as used by Saffman). We also correct several typographical errors of Saffman's paper.

Using Eq. (4), Saffman derives the following relations:

$$\langle u \rangle = \frac{1}{L}\int_{-L/2}^{L/2} u(x)dx = 0, \tag{5}$$

$$u_{\mathrm{rms}} = \sqrt{\langle u^2 \rangle} = \frac{\mu}{\sqrt{12}}, \tag{6}$$

$$\langle \epsilon \rangle = \nu\left\langle \left(\frac{\partial u}{\partial x}\right)^2 \right\rangle = \frac{\mu^3}{12L}, \tag{7}$$

where $\langle u \rangle$, u_{rms}, and $\langle \epsilon \rangle$ are, respectively, the mean velocity, rms velocity, and mean energy dissipation rate. Saffman also derived the second-order structure function as

$$S_2(r) = \langle [u(x+r) - u(x)]^2 \rangle = \frac{\mu^2}{L}\left[r\coth\left(\frac{\mu r}{4\nu}\right) - \frac{4\nu}{\mu}\right]. \tag{8}$$

For small r, using the approximation $\coth x \approx 1/x + x/3$, we derive that

$$S_2(r) \approx \frac{\mu^3 r^2}{12\nu L}. \tag{9}$$

However, for large r, using $\coth x \approx 1$, we deduce that

$$S_2(r) \approx \frac{\mu^2 r}{L}. \tag{10}$$

An important quantity for studying local scaling properties of the structure function is its logarithmic local slope $\zeta_2(r)$, which is defined as (Buzzicotti *et al.* [40])

$$\zeta_2(r) = \frac{d\ \log S_2(r)}{d\ \log r}. \tag{11}$$

The substitution of $S_2(r)$ from Eq. (8) into Eq. (11) leads to the following expression of $\zeta_2(r)$:

$$\zeta_2(r) = \left[\frac{\coth\left(\frac{\mu r}{4\nu}\right) - \frac{\mu r}{4\nu}\,\mathrm{cosech}^2\left(\frac{\mu r}{4\nu}\right)}{\coth\left(\frac{\mu r}{4\nu}\right) - \frac{4\nu}{\mu r}}\right]. \tag{12}$$

Using Eq. (8), we derive

$$\langle u(x+r)u(x)\rangle = \langle u^2\rangle - \frac{1}{2}S_2(r) = \frac{\mu^2}{12} - \frac{\mu^2}{2L}\left[r\coth\left(\frac{\mu r}{4\nu}\right) - \frac{4\nu}{\mu}\right], \tag{13}$$

Hence, the energy spectrum of Burgers turbulence is

$$E(k) = \frac{1}{\pi}\int_0^\infty \langle u(x+r)u(x)\rangle \cos(kr)dr = \frac{2\pi\nu^2}{L}\mathrm{cosech}^2\left(\frac{2\pi\nu k}{\mu}\right). \tag{14}$$

The inertial range corresponds to $2\pi\nu k/\mu \ll 1$. Using $\sinh x \approx x$ for small x, we derive the inertial-range energy spectrum as

$$E(k) = \frac{\mu^2}{2\pi L}k^{-2}. \tag{15}$$

For large x, $\sinh x \approx \exp x$. Using this asymptotic relation we derive the dissipation range $E(k)$ as

$$E(k) = \frac{8\pi\nu^2}{L}\exp\left[-\frac{4\pi\nu k}{\mu}\right]. \tag{16}$$

Interestingly, Saffman's [12] formulas are applicable to the inertial-dissipation range of Burgers turbulence, unlike the majority of earlier works that focused on the inertial range [15,17,23]. Apart from Saffman's work, there are only a small number of works on the dissipation range of Burgers turbulence. Recently, Verma [36] generalized Pao's hypothesis for hydrodynamic turbulence to Burgers turbulence and derived that $E(k) = (\mu^2/L)k^{-2}\exp(-2\nu k/\mu)$. This formula differs from that of Saffman.

In the next subsection, we derive the energy flux using the expression of the energy spectrum [Eq. (14)].

B. Energy flux

The energy flux $\Pi(k_0)$ is defined as the net nonlinear energy transfer from all the modes inside the band $-k_0 \leqslant k' \leqslant k_0$ to the modes outside the band. We compute $\Pi(k_0)$ using the formula ([36,41,42])

$$\Pi(k_0) = -\sum_{|k'|\leqslant k_0} T(k'), \tag{17}$$

where

$$T(k') = \frac{k'}{2}\sum_p \mathrm{Im}[\hat{u}(q)\hat{u}(p)\hat{u}^*(k')]. \tag{18}$$

Here, $q = k' - p$, $\hat{u}(p)$, $\hat{u}(q)$, and $\hat{u}(k')$ are the Fourier amplitudes of the velocity field, and Re, Im, and *, respectively, represent the real part, imaginary part, and complex conjugate of a complex quantity. The energy flux and spectrum are linked to the following dynamical equation [36]:

$$\frac{\partial}{\partial t}E(k) = -\frac{\partial}{\partial k}\Pi(k) - D(k) + \mathcal{F}(k), \tag{19}$$

where $D(k) = 2\nu k^2 E(k)$ and $\mathcal{F}(k) = \Re[\hat{F}(k)\hat{u}^*(k)]$ are, respectively, the energy dissipation rate and the energy injection rate at wave number k. We consider the force $\hat{F}(k)$ to be active at large scales. Hence, the energy injection rate $\mathcal{F}(k) = 0$ in the inertial-dissipation range. In addition, $\partial_t E(k, t) = 0$ for the steady state. Under these conditions, following Eq. (19), we deduce that in the inertial-dissipation range, the energy flux $\Pi(k)$ satisfies the following equation:

$$\frac{d}{dk}\Pi(k) = -D(k) = -2\nu k^2 E(k). \tag{20}$$

In Eq. (20), we substitute $E(k)$ from Eq. (14) and derive

$$\Pi(k) = \frac{\mu^3}{2\pi^2 L}\left[\mathrm{Li}_2\left\{\exp\left(\frac{-4\pi\nu k}{\mu}\right)\right\} - \left(\frac{4\pi\nu k}{\mu}\right)\log\left\{1 - \exp\left(-\frac{4\pi\nu k}{\mu}\right)\right\} - \left(\frac{2\pi\nu k}{\mu}\right)^2\left\{1 - \coth\left(\frac{2\pi\nu k}{\mu}\right)\right\}\right], \tag{21}$$

where

$$\mathrm{Li}_n(z) = \sum_{m=1}^{\infty}\frac{z^m}{m^n}, \tag{22}$$

where $|z| \leqslant 1$ represents the nth-order polylogarithm function [43]. Note that the formulas of Eqs. (8), (14), and (21) are the exact relations that are applicable to the entire range of lengthscales or wave numbers.

In the following subsection, we construct universal functions for the structure function, energy spectrum, and energy flux.

C. Universal functions

The formulas of Eqs. (8), (12), (14), and (21) are complex functions of parameters ν, μ, L, and k. In this subsection, we derive compact relations by nondimensionalizing them. For the same, we employ $r_0 = \nu/\mu$ as the lengthscale and $u_0 = \sqrt{\mu\nu/L}$ as the velocity scale. Note that r_0 is 1/4th of the shock width proposed by Saffman and u_0 is the velocity at small scales. Based on these scales, the nondimensional distance $\tilde{r}$ and wave number $\tilde{k}$ are defined as

$$\tilde{r} = \frac{r}{r_0} = \frac{\mu}{\nu}r, \tag{23}$$

$$\tilde{k} = kr_0 = \frac{\nu}{\mu}k. \tag{24}$$

Using the above scales, we define the nondimensional structure function $\tilde{S}_2(\tilde{r})$, logarithmic local slope $\tilde{\zeta}_2(\tilde{r})$, energy spectrum $\tilde{E}(\tilde{k})$, and energy flux $\tilde{\Pi}(\tilde{k})$ as

$$\tilde{S}_2(\tilde{r}) = \frac{1}{u_0^2} S_2(r) = \frac{L}{\mu\nu} S_2(r) = \tilde{r}\coth\left(\frac{\tilde{r}}{4}\right) - 4, \tag{25}$$

$$\tilde{\zeta}_2(\tilde{r}) = \frac{d\,\log\tilde{S}_2(\tilde{r})}{d\,\log\tilde{r}} = \left[\frac{\coth\left(\frac{\tilde{r}}{4}\right) - \frac{\tilde{r}}{4}\,\mathrm{cosech}^2\left(\frac{\tilde{r}}{4}\right)}{\coth\left(\frac{\tilde{r}}{4}\right) - \frac{4}{\tilde{r}}}\right], \tag{26}$$

$$\tilde{E}(\tilde{k}) = \frac{1}{u_0^2 r_0} E(k) = \frac{L}{\nu^2} E(k) = 2\pi\,\mathrm{cosech}^2(2\pi\tilde{k}), \tag{27}$$

$$\begin{aligned}\tilde{\Pi}(\tilde{k}) &= \frac{r_0}{u_0^3}\Pi(k) = \sqrt{\mathrm{Re}}\,\frac{L}{\mu^3}\Pi(k)\\ &= \frac{\sqrt{\mathrm{Re}}}{2\pi^2}[\mathrm{Li}_2\{\exp(-4\pi\tilde{k})\} - 4\pi\tilde{k}\log\{1-\exp(-4\pi\tilde{k})\}\\ &\quad - (2\pi\tilde{k})^2\{1-\coth(2\pi\tilde{k})\}].\end{aligned} \tag{28}$$

In the inertial range (large $\tilde{r}$), Eqs. (25) and (27) transform to

$$\tilde{S}_2(\tilde{r}) = \tilde{r} \quad \text{and} \quad \tilde{E}(\tilde{k}) = \frac{1}{2\pi}\tilde{k}^{-2}. \tag{29}$$

In the dissipation range ($\tilde{r} \lessapprox 1$), the structure function and energy spectrum are

$$\tilde{S}_2(\tilde{r}) = \tfrac{1}{12}\tilde{r}^2 \quad \text{and} \quad \tilde{E}(\tilde{k}) = 8\pi\,\exp[-4\pi\tilde{k}]. \tag{30}$$

In addition, it can be shown that in the inertial range

$$\tilde{\Pi}(\tilde{k}) = \frac{1}{12}\sqrt{\mathrm{Re}}, \tag{31}$$

which is consistent with the fact that the maximum value of the energy flux $\Pi_{\max} = \langle\epsilon\rangle = \mu^3/12L$ [see Eq. (7)].

The functions $\tilde{S}_2(\tilde{r})$, $\tilde{E}(\tilde{k})$, and $\tilde{\Pi}(\tilde{k})/\sqrt{\mathrm{Re}}$ given above are functions of $\tilde{r}$ and $\tilde{k}$, not of ν and μ. Hence they are universal functions. In Sec. IV, we show that the structure functions, energy spectra, and energy fluxes of many runs collapse to these universal functions. We describe our numerical procedure in the following section.

III. NUMERICAL PROCEDURE

We numerically solve the Burgers equation, Eq. (2), with large-scale forcing. We consider a periodic domain of size $L = 2\pi$. We employ a pseudospectral method for our simulation, and two-third rule for dealiasing. We apply the forcing $\hat{F}(k)$ in such a way that the energy supply rate

$$\epsilon_{\mathrm{inj}} = \sum_k \mathrm{Re}[\hat{F}(k)\hat{u}^*(k)] \tag{32}$$

is constant. Following Stepanov and Plunian [44], we employ

$$\hat{F}(k) = \frac{\epsilon_{\mathrm{inj}}}{n_f[|\hat{u}(k)|\cos(\phi_k - \theta_k)]}\exp(i\phi_k), \tag{33}$$

where n_f is the total number of forcing modes and θ_k and ϕ_k represent the phases of $\hat{u}(k)$ and $\hat{F}(k)$, respectively. We choose random ϕ_k from the uniform distribution in the interval $(0, 2\pi)$. The forcing wave-number band is $|k_f| \in [1, 3]$, hence $n_f = 6$.

We carry out nine numerical runs whose parameters are listed in Table I. The energy supply rate varies from 0.1 to 1, while ν from 10^{-4} to 10^{-3}. All the runs have grid size $N = 2^{16}$, except for Run 5 which has $N = 2^{18}$. We employ the fourth-order Runge-Kutta scheme for time advancement with

TABLE I. The parameters used in our simulations: Grid size N; energy supply rate ϵ_{inj}; kinematic viscosity ν; and Reynolds number $\text{Re} = \mu L/\nu$.

Run	N	ϵ_{inj}	ν	Re
1	2^{16}	1.00	1.0×10^{-3}	2.65×10^{4}
2	2^{16}	1.00	7.5×10^{-4}	3.54×10^{4}
3	2^{16}	1.00	5.0×10^{-4}	5.31×10^{4}
4	2^{16}	1.00	2.5×10^{-4}	1.06×10^{5}
5	2^{18}	1.00	1.0×10^{-4}	2.66×10^{5}
6	2^{16}	0.75	5.0×10^{-4}	4.82×10^{4}
7	2^{16}	0.50	5.0×10^{-4}	4.21×10^{4}
8	2^{16}	0.25	5.0×10^{-4}	3.34×10^{4}
9	2^{16}	0.10	5.0×10^{-4}	2.46×10^{4}

constant time step $\delta t = 5.0 \times 10^{-5}$ for all the runs, except for Run 5 for which $\delta t = 2.5 \times 10^{-5}$. We start the runs with Gaussian-random velocity field with zero mean and a standard deviation of 1.5. We perform all our simulations until $t = 100$. We observe transients during the early stages, after which the system reaches a steady state. In Sec. IV, we report our results, primarily the universal functions, for the steady state.

IV. NUMERICAL VERIFICATION OF UNIVERSAL FUNCTIONS

In this section, we numerically verify the properties of global quantities, the dissipation rate, and rms velocity, as well as the universal functions, such as structure function, energy spectrum, and energy flux.

A. Global quantities

In this subsection, we present the numerical results on global quantities—the mean energy dissipation rate, rms velocity, and the strength of the shock.

The energy supplied at large scales cascades to the smaller scales and eventually gets dissipated by the viscous effects. The instantaneous energy dissipation rate $\epsilon(t)$ is determined by summing

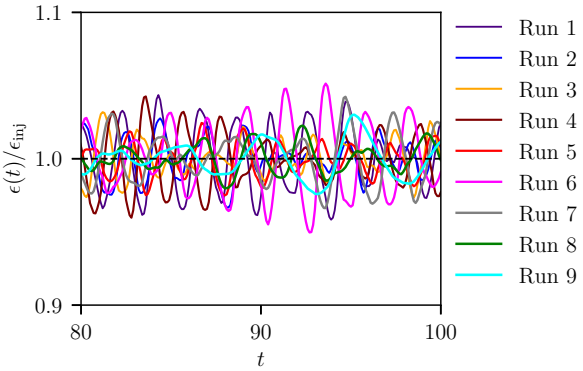

FIG. 2. Plots exhibiting the time evolution of the normalized energy dissipation rate for the steady states. The horizontal dashed line represents $\langle\epsilon\rangle/\epsilon_{\text{inj}} = 1.0$.

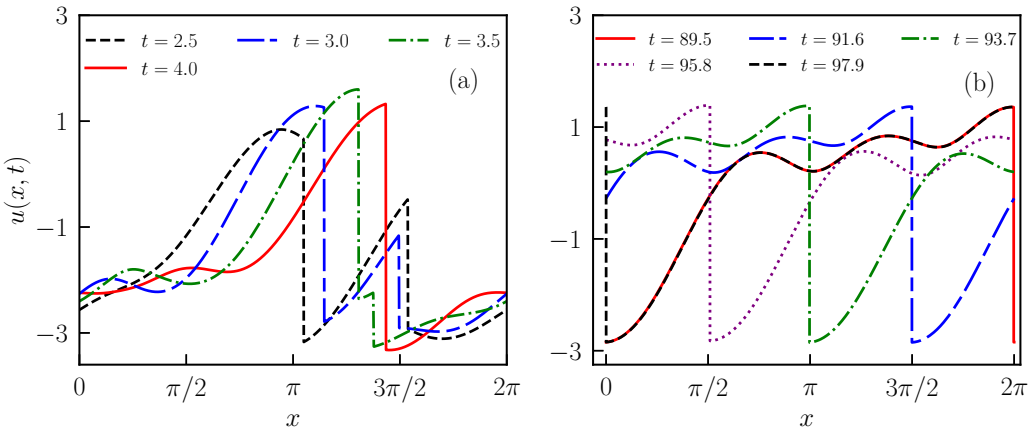

FIG. 3. Plot of exhibiting the velocity field $u(x,t)$ (a) in the transient period in the time interval [2.5, 4.0] and (b) at steady state in the time interval [89.5, 97.9] for Run 5.

$D(k)$ for all k's:

$$\epsilon(t) = \sum_k D(k). \tag{34}$$

In Fig. 2, we exhibit the time series of the normalized dissipation rate $\epsilon(t)/\epsilon_{\text{inj}}$ during the steady state. We observe that $\langle\epsilon\rangle \approx \epsilon_{\text{inj}}$.

Figure 3 illustrates the time series of the velocity field in the transient period and at a steady state for Run 5. As shown in Fig. 3(a), we observe that the velocity field exhibits two shocks in the transient period. These shocks move towards each other as time passes, and eventually merge together and create a single large shock. We demonstrate the merging process of the shocks in Fig. 3(a). Murray and Bustamante [20] also observed a similar merging process which results in the formation of a single large shock. At steady state, Fig. 3(b) shows that the large shock moves leftward with a constant velocity. We note that the steady-state velocity profile of our results is different from that reported in Buzzicotti *et al.* [40]. We believe that it is possibly because of the difference in the forcing used for supplying energy into the system. As shown in Fig. 3(b), u at $t =$

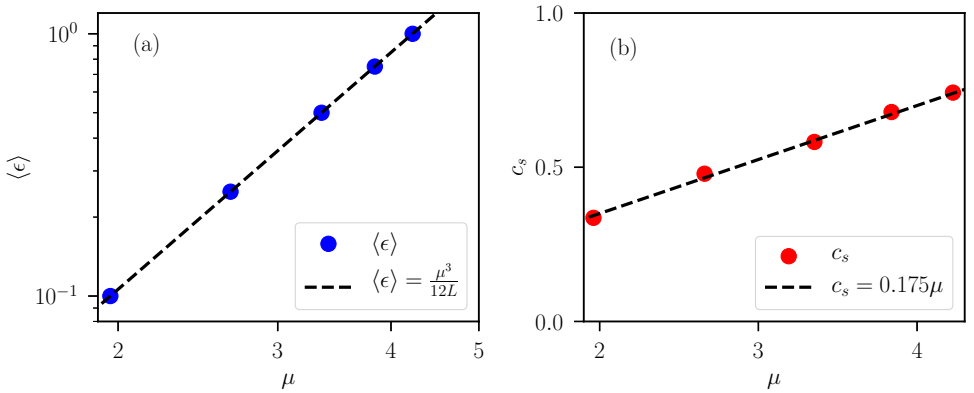

FIG. 4. Plots of the (a) dissipation rate $\langle\epsilon\rangle$ and (b) shock-front velocity c_s as a function of the shock strength μ.

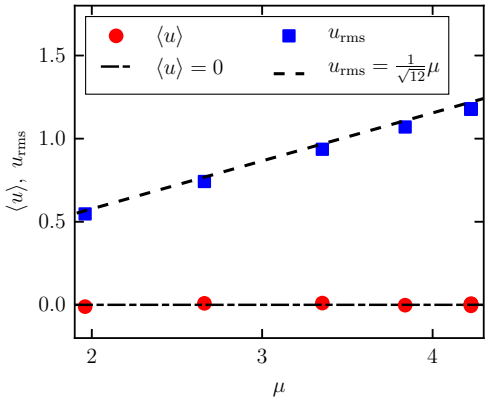

FIG. 5. Plot of the mean velocity $\langle u \rangle$ and rms velocity $u_{\rm rms}$ as a function of the shock strength μ.

89.5 and at $t = 97.6$ overlap with each other. Hence, the speed of the shock front is $c_s \approx 2\pi/8.4 \approx 0.75$ units. A more formal way to compute c_s and μ are ([13,15])

$$c_s = \left| \frac{1}{n} \sum_{i=1}^{n} \left[\frac{\max[u(x,t_i)] + \min[u(x,t_i)]}{2} \right] \right|, \tag{35}$$

$$\mu = \frac{1}{n} \sum_{i=1}^{n} \{\max[u(x,t_i)] - \min[u(x,t_i)]\}, \tag{36}$$

where n is the number of frames used for averaging (here $n = 500$). Note that the error, which is estimated using the standard deviation with respect to the mean, is less than 0.04 for μ and 0.02 for c_s for all the runs.

In Fig. 4, we plot $\langle \epsilon \rangle$ and c_s against μ. As shown in Fig. 4(a), our results verify the relation $\langle \epsilon \rangle = \mu^3/12L$ derived by Saffman [see Eq. (7)]. Figure 4(b) illustrates a linear relationship between the shock-front velocity c_s and the shock strength μ, in particular, $c_s = 0.175\mu$. Note that both μ

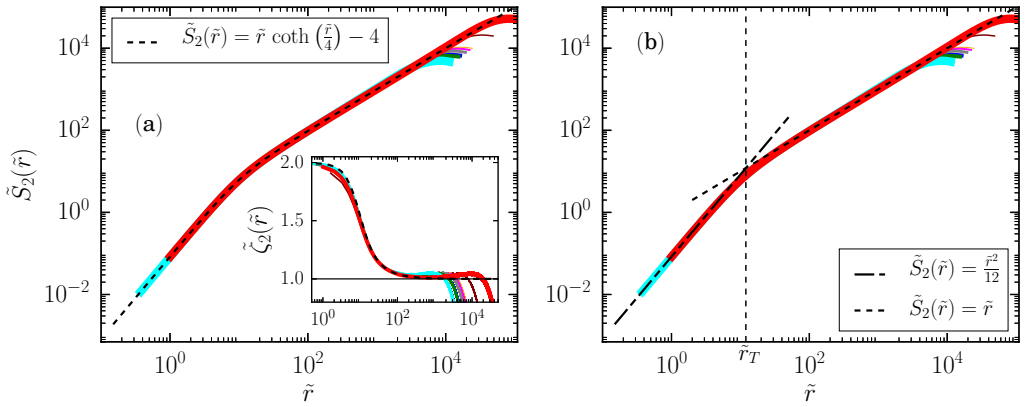

FIG. 6. Plots of the numerically and theoretically computed universal structure function $\tilde{S}_2(\tilde{r})$ and their associated logarithmic local slopes $\tilde{\zeta}_2(\tilde{r})$ [inset of (a)]. Note that the legend for numerical $\tilde{S}_2(\tilde{r})$ and $\tilde{\zeta}_2(\tilde{r})$ are the same as that of Fig. 2. The black dashed line in the inset of (a) represents theoretical $\tilde{\zeta}_2(\tilde{r})$ of Eq. (26).

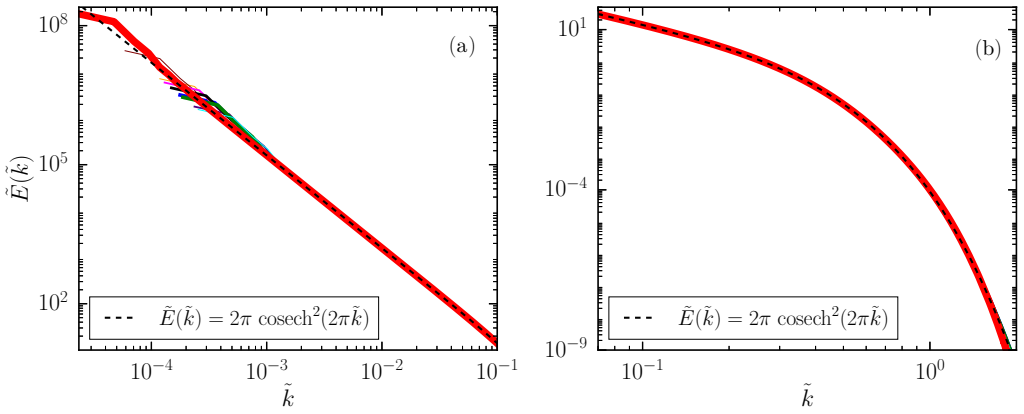

FIG. 7. Plots of (a) the energy spectrum $\tilde{E}(\tilde{k})$ in (a) the inertial range ($\tilde{k} < \tilde{k}_T$) and (b) the dissipation range ($\tilde{k} > \tilde{k}_T$). Legend for numerically computed results is same as that of Fig. 2.

and c_s are independent of viscosity. We also compute the mean velocity $\langle u \rangle$ and rms velocity $u_{\rm rms}$ and plot them against μ in Fig. 5. As shown in the figure, the numerically computed $\langle u \rangle$ and $u_{\rm rms}$ are in agreement with their values calculated using theoretically derived formulas by Saffman [12] [see Eqs. (5) and (6)].

B. Structure function

We numerically compute $\tilde{S}_2(\tilde{r})$ for all the run, and plot them in Fig. 6. We observe that $\tilde{S}_2(\tilde{r})$ for various runs collapse to a single curve and the universal $\tilde{S}_2(\tilde{r})$ of Eq. (25) describes the numerical curve very well, except for large $\tilde{r}$ [see Fig. 6(a)]. The discrepancy at large $\tilde{r}$ occurs due to the large-scaling forcing, which is not universal. We also plot $\tilde{\zeta}_2(\tilde{r})$ in the inset of Fig. 6(a). As shown in the figure, the numerically computed $\tilde{\zeta}_2(\tilde{r})$ of all the runs follows the universal $\tilde{\zeta}_2(\tilde{r})$ of Eq. (26) very well. In addition, we observe that $\tilde{\zeta}_2(\tilde{r}) \approx 2$ in the dissipation range and $\tilde{\zeta}_2(\tilde{r}) \approx 1$ in the inertial range. Also, the overall variation of $\tilde{\zeta}_2(\tilde{r})$ is consistent with that reported in Fig. 3(a) of Buzzicotti *et al.* [40]. However, one major difference is that Buzzicotti et al.'s [40] results showed $\tilde{\zeta}_2(\tilde{r}) < 1$ in the inertial range and this is because their results were for the decimated Burgers equation. In

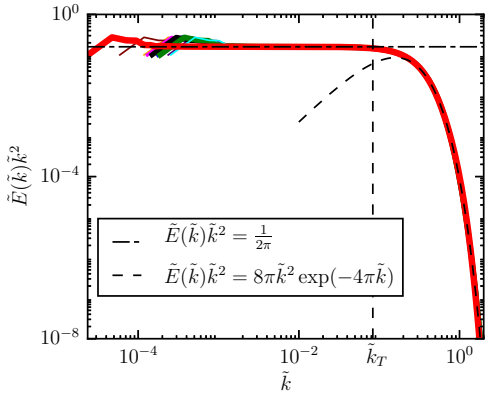

FIG. 8. Plots of the normalized energy spectrum $\tilde{E}(\tilde{k})\tilde{k}^2$. Legend for numerically computed results is the same as that of Fig. 2.

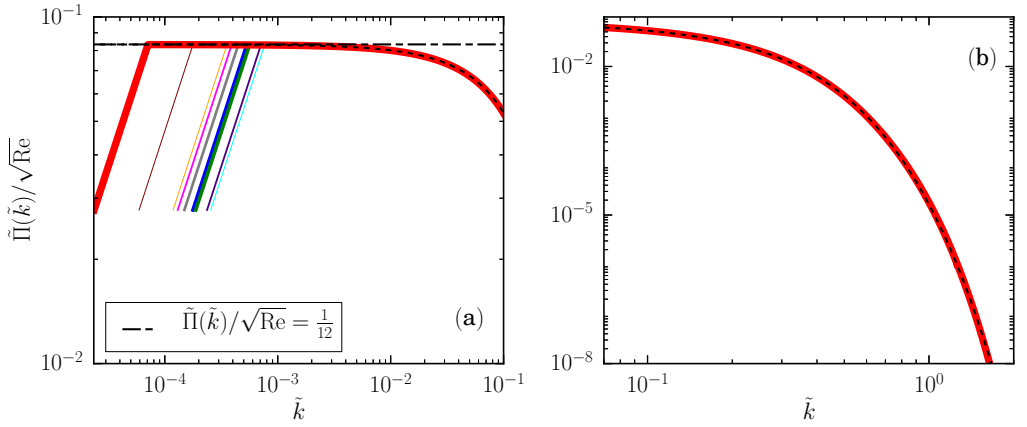

FIG. 9. Plots of the normalized energy flux $\tilde{\Pi}(\tilde{k})/\sqrt{\mathrm{Re}}$ in (a) the inertial range ($\tilde{k} < \tilde{k}_T$) and (b) the dissipation range ($\tilde{k} > \tilde{k}_T$). Legend for numerically computed results is same as that of Fig. 2. The black dashed lines in (a,b) represent theoretical $\tilde{\Pi}(\tilde{k})/\sqrt{\mathrm{Re}}$ of Eq. (28).

Fig. 6(b), we compare the numerical results with the theoretical predictions that $\tilde{S}_2(\tilde{r}) = \tilde{r}$ and $\tilde{S}_2(\tilde{r}) = \tilde{r}^2/12$ in the inertial and dissipation ranges, respectively [see Eqs. (29) and (30). We observe good agreement between the theoretical and numerical results. Note that the transition between the two regimes occurs near $\tilde{r} = \tilde{r}_T = 12$.

C. Spectral quantities

Here we compare the numerical results on energy spectrum and flux with the corresponding universal functions.

We numerically compute $\tilde{E}(\tilde{k})$ for all the runs and plot the inertial range regime of the computed $\tilde{E}(\tilde{k})$ in Fig. 7(a) and dissipation range regime in Fig. 7(b). The figure shows that $\tilde{E}(\tilde{k})$ for all the runs collapses to a single curve in the inertial-dissipation range, and the collapsed curve matches with the universal curve for the energy spectrum [Eq. (27)] quite well. In addition, as shown in Fig. 8, $\tilde{E}(\tilde{k}) = 1/(2\pi k^2)$ for the inertial range, while $\tilde{E}(\tilde{k}) = 8\pi \exp(-4\pi\tilde{k})$ in the dissipation range are acceptable approximations. The transition between the two regimes occurs near $\tilde{k} = \tilde{k}_T = 1/\tilde{r}_T = 1/12$. These results are consistent with Eqs. (29) and (30). Note that the difference in Girimaji and Zhou's [29] numerical results and Saffman's predictions was due to the typographical error in Saffman's formula. We also compute $\tilde{\Pi}(\tilde{k})/\sqrt{\mathrm{Re}}$ for all the runs. We plot the inertial range regime of $\tilde{\Pi}(\tilde{k})/\sqrt{\mathrm{Re}}$ in Fig. 9(a) and dissipation range regime in Fig. 9(b). The figure shows that the fluxes of various runs collapse to a single curve, except at small $\tilde{k}$ due to the forcing function at large scale. In addition, the collapsed curve is in good agreement with the universal function of Eq. (28). Also, for the inertial range, $\tilde{\Pi}(\tilde{k})/\sqrt{\mathrm{Re}} = 1/12$ or $\Pi_{\max} = \mu^3/12L = \epsilon_{\mathrm{inj}} = \langle\epsilon\rangle$, consistent with Eq. (7).

Thus, we verify the applicability of the universal functions of the structure function, energy spectrum, and energy flux for the forced Burgers equation. We conclude the paper in Sec. V.

V. CONCLUSION

Saffman [12] derived an analytical solution for forced Burgers turbulence in the asymptotic limit of $\nu \to 0$ and $t \to \infty$. Using the solution, he computed u_{rms}, the average dissipation rate, as well as the structure function and energy spectrum for the Burgers equation. In this paper, we compute the energy flux using Saffman's energy spectrum. The energy flux, energy spectrum, and structure function describe the inertial and dissipative ranges of Burgers turbulence. This is remarkable because most works on Burgers turbulence focus on the inertial range only.

Saffman's formulas are complex functions of ν, μ, L, r, and k. In this paper, we nondimensionalize these formulas and derive universal functions. To verify these universal functions, we simulate the Burgers equation for different parameters. We force the equation with large-scale random forcing. We observe that the numerical results collapse to the respective universal functions, except at large length scales, which is due to the forcing.

Saffman's formulas and the corresponding universal functions are important advance in the field. For many years, researchers have been attempting to construct the inertia-dissipation energy spectrum for hydrodynamic turbulence. The proposed dissipation-range spectra are $\exp(-k)$, $\exp(-k^{2/3})$, $\exp(-k^{4/3})$, and $\exp(-k^2)$, but there is no convergence at this stage (e.g., see [45–48]). We believe that Saffman's successful model may provide valuable ideas for modeling the inertial-dissipation range of hydrodynamic turbulence.

ACKNOWLEDGMENTS

We thank Soumyadeep Chatterjee, Mohammad Anas, and Roshan Samuel for useful discussions. M.K.V. and P.K.S. gratefully acknowledge financial support from the Science and Engineering Research Board (SERB), India for the research grant (Grant No. TAR/2018/000150) under the Teachers Associateship for Research Excellence (TARE). Our numerical simulations were performed on HPC2013 and the Taylor cluster of IIT Kanpur, India.

[1] J. M. Burgers, *A Mathematical Model Illustrating the Theory of Turbulence*, Advances in Applied Mechanics, (Elsevier, Amsterdam, 1948), pp. 171–199.
[2] J. M. Burgers, *The Nonlinear Diffusion Equation: Asymptotic Solutions and Statistical Problems* (Springer Science & Business Media, New York, 2013).
[3] J. M. Burgers, *Selected Papers of J. M. Burgers* (Springer, Dordrecht, The Netherlands, 1995), p. 281.
[4] D. Chowdhury, L. Santen, and A. Schadschneider, Statistical physics of vehicular traffic and some related systems, Phys. Rep. **329**, 199 (2000).
[5] S. N. Gurbatov and A. I. Saichev, Degeneracy of one-dimensional acoustic turbulence under large Reynolds numbers, Zh. Éksp. Teor. Fiz. **80**, 689 (1981) [Sov. Phys. JETP **53**, 347 (1981)].
[6] S. N. Gurbatov, A. I. Saichev, and I. G. Yakushkin, Nonlinear waves and one-dimensional turbulence in nondispersive media, Sov. Phys. Usp. **26**, 857 (1983).
[7] S. N. Gurbatov, I. Y. Demin, and A. I. Saichev, Establishment of self-similar regimes of nonlinear random waves in dissipative media, Zh. Éksp. Teor. Fiz. **87**, 497 (1984) [Sov. Phys. JETP **60**, 284 (1984)].
[8] Ş. A. Büyükaşık and O. K. Pashaev, Exact solutions of forced Burgers equations with time variable coefficients, Commun. Nonlinear Sci. Numer. Simul. **18**, 1635 (2013).
[9] P. Gupta and C. Scalo, Spectral energy cascade and decay in nonlinear acoustic waves, Phys. Rev. E **98**, 033117 (2018).
[10] A. Cordero, A. Franques, and J. R. Torregrosa, Numerical solution of turbulence problems by solving Burgers' equation, Algorithms **8**, 224 (2015).
[11] J. Bec and K. Khanin, Burgers turbulence, Phys. Rep. **447**, 1 (2007).
[12] P. G. Saffman, in *Topics in Nonlinear Physics*, edited by N. J. Zabusky (Springer, Berlin, 1968), pp. 485–614.
[13] T. Tatsumi and S. Kida, Statistical mechanics of the Burgers model of turbulence, J. Fluid Mech. **55**, 659 (1972).
[14] J. M. Burgers, *The Nonlinear Diffusion Equation* (D. Reidel, Dordrecht, The Netherlands, 1974).
[15] S. Kida, Asymptotic properties of Burgers turbulence, J. Fluid Mech. **93**, 337 (1979).
[16] T. Gotoh and R. H. Kraichnan, Statistics of decaying Burgers turbulence, Phys. Fluids **5**, 445 (1993).
[17] M. K. Verma, Intermittency exponents and energy spectrum of the Burgers and KPZ equations with correlated noise, Physica A **277**, 359 (2000).

[18] S. N. Gurbatov, S. I. Simdyankin, E. Aurell, U. Frisch, and G. Toth, On the decay of Burgers turbulence, J. Fluid Mech. **344**, 339 (1997).
[19] J. Bec, U. Frisch, and K. Khanin, Kicked Burgers turbulence, J. Fluid Mech. **416**, 239 (2000).
[20] B. P. Murray and M. D. Bustamante, Energy flux enhancement, intermittency and turbulence via Fourier triad phase dynamics in the 1-D Burgers equation, J. Fluid Mech. **850**, 624 (2018).
[21] K. Ohkitani and M. Dowker, Numerical study on comparison of Navier-Stokes and Burgers equations, Phys. Fluids **24**, 055113 (2012).
[22] C. V. Tran and D. G. Dritschel, Energy dissipation and resolution of steep gradients in one-dimensional Burgers flows, Phys. Fluids **22**, 037102 (2010).
[23] T. Gotoh, Inertial range statistics of Burgers turbulence, Phys. Fluids **6**, 3985 (1994).
[24] J. P. Bouchaud, M. Mézard, and G. Parisi, Scaling and intermittency in Burgers turbulence, Phys. Rev. E **52**, 3656 (1995).
[25] A. Chekhlov and V. Yakhot, Kolmogorov turbulence in a random-force-driven Burgers equation, Phys. Rev. E **51**, R2739 (1995).
[26] F. Hayot and C. Jayaprakash, Multifractality in the stochastic Burgers equation, Phys. Rev. E **54**, 4681 (1996).
[27] J. Fleischer and P. H. Diamond, Burgers' turbulence with self-consistently evolved pressure, Phys. Rev. E **61**, 3912 (2000).
[28] Z.-X. Zhang and Z.-S. She, Subensemble decomposition and Markov process analysis of Burgers turbulence, Phys. Rev. E **84**, 026326 (2011).
[29] S. S. Girimaji and Y. Zhou, Spectrum and energy transfer in steady Burgers turbulence, Phys. Lett. A **202**, 279 (1995).
[30] A. Das and R. D. Moser, Optimal large-eddy simulation of forced Burgers equation, Phys. Fluids **14**, 4344 (2002).
[31] Q. Ni, Y. Shi, and S. Chen, Statistics of one-dimensional compressible turbulence with random large-scale force, Phys. Fluids **25**, 075106 (2013).
[32] S. Moradi, B. Teaca, and J. Anderson, Role of phase synchronisation in turbulence, AIP Adv. **7**, 115213 (2017).
[33] M. Buzzicotti, B. P. Murray, L. Biferale, and M. D. Bustamante, Phase and precession evolution in the Burgers equation, Eur. Phys. J. E **39**, 34 (2016).
[34] S. L. Shalimov, Short-wavelength asymptotic behavior of the Burgers turbulence spectrum, Jetp Lett. **67**, 405 (1998).
[35] Y.-H. Pao, Structure of turbulent velocity and scalar fields at large wavenumbers, Phys. Fluids **8**, 1063 (1965).
[36] M. K. Verma, *Energy Transfers in Fluid Flows: Multiscale and Spectral Perspectives* (Cambridge University Press, Cambridge, England, 2019).
[37] S. S. Ray, U. Frisch, S. V. Nazarenko, and T. Matsumoto, Resonance phenomenon for the Galerkin-truncated Burgers and Euler equations, Phys. Rev. E **84**, 016301 (2011).
[38] S. D. Murugan, U. Frisch, S. Nazarenko, N. Besse, and S. S. Ray, Suppressing thermalization and constructing weak solutions in truncated inviscid equations of hydrodynamics: Lessons from the Burgers equation, Phys. Rev. Research **2**, 033202 (2020).
[39] M. K. Verma, S. Chatterjee, A. Sharma, and A. Mohapatra, Equilibrium states of Burgers and Korteweg–de Vries equations, Phys. Rev. E **105**, 034121 (2022).
[40] M. Buzzicotti, L. Biferale, U. Frisch, and S. S. Ray, Intermittency in fractal Fourier hydrodynamics: Lessons from the Burgers equation, Phys. Rev. E **93**, 033109 (2016).
[41] M. K. Verma, Statistical theory of magnetohydrodynamic turbulence: recent results, Phys. Rep. **401**, 229 (2004).
[42] M. K. Verma, Variable energy flux in turbulence, J. Phys. A: Math. Theor. **55**, 013002 (2022).
[43] L. Lewin, *Structural Properties of Polylogarithms*, Mathematical Surveys and Monographs (American Mathematical Society, Providence, RI, 1991).
[44] R. Stepanov and F. Plunian, Fully developed turbulent dynamo at low magnetic Prandtl numbers, J. Turbul. **7**, N39 (2006).

[45] S. Chen, G. Doolen, J. R. Herring, R. H. Kraichnan, S. A. Orszag, and Z. S. She, Far-dissipation range of turbulence, Phys. Rev. Lett. **70**, 3051 (1993).
[46] T. Sanada, Comment on the dissipation-range spectrum in turbulent flows, Phys. Fluids **4**, 1086 (1992).
[47] D. Buaria and K. R. Sreenivasan, Dissipation range of the energy spectrum in high Reynolds number turbulence, Phys. Rev. Fluids **5**, 092601(R) (2020).
[48] M. K. Verma, A. Kumar, P. Kumar, S. Barman, A. G. Chatterjee, R. Samtaney, and R. Stepanov, Energy spectra and fluxes in dissipation range of turbulent and laminar flows, Fluid Dyn. **53**, 862 (2018).